Impacts of climate change on volcanic stratospheric injections: comparison of 1D and 3D plume model projections

T. J. Aubry[1*], M. Cerminara[2] and A. M. Jellinek[3]

[1]University of Cambridge, Department of Geography, Cambridge, United Kingdom
[2]National Institute of Geophysics and Volcanology, Pisa, Italy
[3]University of British Columbia, Department of Earth, Ocean and Atmospheric Sciences, Vancouver, Canada

Key Points:

- We compare the impacts of climate change on the dynamics of eruptive columns, as predicted by 1D and 3D plume models.
- Both models agree that higher eruption intensities will be required to inject sulfur into the tropical stratosphere.
- Eruptive column-climate interactions are key to understand the climatic impacts of future eruptions.

*Previously at University of British Columbia, Department of Earth, Ocean and Atmospheric Sciences, Vancouver, Canada

Corresponding author: Thomas J. Aubry, ta460@cam.ac.uk

Abstract

Explosive volcanic eruptions are one of the most important driver of climate variability. Yet, we still lack a fundamental understanding of how climate change may affect future eruptions. Here, we use an ensemble of simulations by 1D and 3D volcanic plume models spanning a large range of eruption source and atmospheric conditions to assess changes in the dynamics of future eruptive columns. Our results shed new light on differences between the predictions of 1D and 3D plume models. Furthermore, both models suggest that as a result of ongoing climate change, for tropical eruptions: i) higher eruption intensities will be required for plumes to reach the upper troposphere/lower stratosphere (UTLS); and ii) the height of plumes currently reaching the UTLS or above will increase. We discuss the implications of these results for the climatic impacts of future eruptions. Our simulations can directly inform climate model experiments on climate-volcano feedback.

1 Introduction

Explosive volcanic eruptions that inject sulfur gases into the stratosphere modulate Earth's radiative balance and are a major natural climate forcing (e.g. Robock (2000); Sigl et al. (2015)). Large volcanic eruptions (e.g. Mt. Tambora 1815, Mt. Pinatubo 1991) result in global mean surface cooling of the order of 0.5-1 K. Smaller and more frequent volcanic events also have a significant climate footprint and have offset 30% of anthropogenic CO_2 forcing over 2000-2015 (e.g. Santer et al. (2014); Schmidt et al. (2018)).

Conversely, climate can affect volcanoes. In particular, the impacts of glaciation/deglaciation cycles on the frequency of volcanic eruptions has been the focus of many studies (e.g. Jellinek et al. (2004); Watt et al. (2013); Cooper et al. (2018)). However, the exploration of climate-volcano feedback related to processes governing the climatic impact of a volcanic eruption is nascent. For example, changes in ocean stratification (Fasullo et al., 2017) and tropospheric aerosols (Hopcroft et al., 2017) are expected to affect the climate response to future eruptions. Despite the widely studied sensitivity of volcanic plume dynamics to atmospheric conditions (e.g. Woods (1995); Bursik (2001); Costa et al. (2016) and references therein), a single study has investigated the impact of global warming on plume rise and subsequent atmospheric SO_2 injections: Using a one-dimensional integral (1D) model of volcanic plume (Degruyter & Bonadonna, 2012), Aubry et al. (2016) suggest that global warming will result in decreased volcanic stratospheric sulfate injections in the tropics as a consequence of projected changes in temperature profiles. To quantify the amount of gas injected into the stratosphere for specified eruption source and atmospheric conditions, the vertical distribution of mass flux from the plume to the umbrella cloud is required. We briefly review the dynamics governing this distribution hereafter.

During an explosive eruption, hot volcanic gases and particles are released from the vent into the atmosphere forming a turbulent, multiphase flow. Turbulence induces mixing with the surrounding atmosphere, which is entrained into the rising gas-particle mixture, affecting the plume buoyancy (Morton et al., 1956; Morton, 1959). Entrainment thus control the neutral buoyancy level (NBL) (Woods, 1988; Cerminara, Ongaro, & Neri, 2016) above which an umbrella cloud spreads, injecting ash and gas into the atmosphere (Suzuki & Koyaguchi, 2009; Devenish & Cerminara, 2018). 1D plume models represent entrainment as an inflow of atmosphere into the plume characterized by an entrainment velocity (u_ϵ on Fig. 1). This velocity is parameterized as a function of the averaged plume velocity and horizontal wind speed, through two empirically constrained entrainment coefficients that are subject to high uncertainties (Aubry et al. (2017) and references herein). On the other hand, 3-dimensional (3D) plume models resolve the multiphase Navier Stokes equations and turbulence down to grid scale (Large Eddy Simulations, LES). Some of them need an empirical parameter for the sub-grid turbulence (Smagorinsky, 1963), others use dynamic LES and do not need any parameters (Bardina et al., n.d.; Moin et al., 1991; Cerminara, Ongaro, & Berselli, 2016; Cerminara, Ongaro, & Neri, 2016). These different approaches are the main cause of differences in plume height predictions among 3D and 1D models (Costa et al., 2016).

Another key difference between 1D and 3D model is that 1D plume models rely on a self-similarity assumption prescribing the distribution of gas, particles, and velocity fields across any section of the plume (e.g. "top-hat profile", Fig. 1). 1D models thus cannot directly predict the vertical injection profile, but only the plume height, either defined as the NBL or the top height, which differ by 25-50%. Furthermore, the umbrella cloud is characterized by lateral intrusions into the atmosphere and downward flow from the region overshooting the NBL. Consequently, the self-similarity assumption in 1D models is violated above the NBL resulting in unreliable top height predictions.

As a consequence of the limitations of 1D models in predicting a full injection profile for volcanic gases, it is critical to investigate how climate change will affect volcanic plume dynamics using 3D models. In particular, how would the feedback hypothesis of Aubry et al. (2016) - decreased stratospheric volcanic inputs in a warmer world - be modified if investigated with a 3D plume model? To answer these questions, we conduct a suite of benchmark numerical experiments to compare the projections of the 1D plume model used by Aubry et al. (2016) with a 3D plume model (Cerminara, Ongaro, & Berselli, 2016; Cerminara, Ongaro, & Neri, 2016). In addition to refining predictions for the fate of volcanic plume dynamics on a warming Earth, our results provide valuable insights on differences between 1D and 3D plume models.

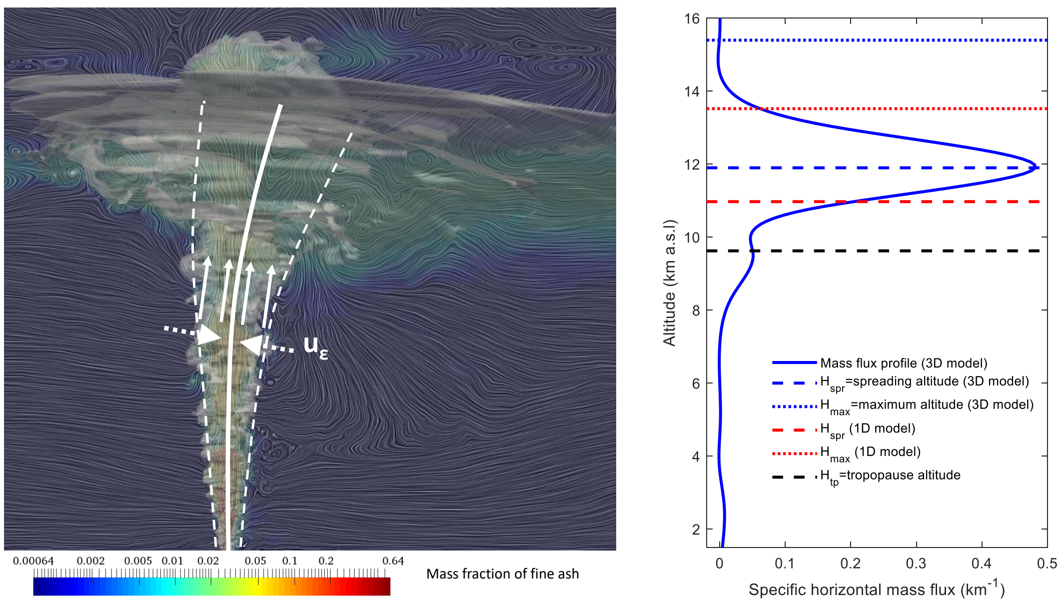

Figure 1. Left: Fields of one of the 3D plume model simulation. Dark blue and white shadings show streamlines of the instantaneous velocity field. The grey shading shows the area where the instantaneous fine ash content is above 1% of that at the vent. The color shading show the instantaneous fine ash fraction. Thick white lines show the centerline and plume radius of the corresponding 1D simulation, with arrows illustrating the top-hat velocity profile used and entrainment velocity u_ϵ.
Right: Time-averaged specific mass flux profile of the 3D model for the simulation shown in the left panel. Horizontal lines show the spreading and top heights of the 1D and 3D models as well as the tropopause height.

2 Volcanic plume models

For the 1D plume model, we use the model described in Degruyter and Bonadonna (2012), which was also adopted by Aubry et al. (2016). Radial profiles of plume properties are assumed to be self-similar (of top-hat shape) along the plume centerline and are integrated to obtain fluxes of mass, momentum and heat, which are then assumed to be conserved along the plume centerline (Fig. 1). The turbulent entrainment of atmosphere into the plume is parameterized following Hoult et al. (1969) and the condensation of water vapor in the plume following Glaze et al. (1997). Parameter values are chosen to produce the best agreement between the 1D and 3D plume model for NBL predictions, for late 20$^{\text{th}}$ century climate conditions (cf. section 3):

- Entrainment coefficient are constants, with a value of 0.06 for the radial entrainment coefficient and 0.15 for the wind entrainment coefficient.
- The condensation rate is 10^{-6} s^{-1}, for which condensation of water vapor in the plume has negligible effects on plume height.

These values are close to those found to produce the best agreement with an eruption source parameter database of 94 eruptive events (Aubry & Jellinek, 2018). We assume that the NBL predicted by the 1D model is representative of the height of spreading of the umbrella cloud. Our 3D model simulations show that this assumption is fairly reasonable, with the two heights being extremely well correlated ($R^2 = 0.96$), but the NBL being $\simeq 15\%$ smaller than the spreading height.

For the 3D plume model, we use ASHEE, the 3D model presented in Cerminara, Ongaro, and Neri (2016) and Cerminara, Ongaro, and Berselli (2016). ASHEE solves the compressible fluid dynamics of turbulent multiphase flows. Turbulence is treated via the dynamic Large Eddy Simulations method. Decoupling between gas and solid phases can be treated with a combined Eulerian-Lagrangian approach but is kept switched-off in this study to obtain results independent from the grain-size distribution. However, we have checked that kinematic decoupling of pyroclasts is not influencing much the mass distribution of gas and fine ash (< 64 microns) in the umbrella cloud (Fig. S1). The distribution of volcanic ash and gas in the umbrella cloud are extracted from the 3D model using an averaging technique based on the vertical evolution of the plume mass flow rate. The maximum spreading level is obtained from these profiles, as the level where the injection flow is maximum. The duration of all 3D simulations is 2000 s, enough to define stable time-averaged quantities in the time window 1000-2000 s from the eruption start.

3 Design of numerical experiments

Both 1D and 3D volcanic plume models require two types of inputs: eruption source parameters and atmospheric conditions.

The only source parameter we varied in our numerical experiments is the mass eruption rate (MER, also called eruption intensity), for which we tested 10 values regularly spaced on a logarithmic scale between 1.6×10^5 and 7.9×10^7 kg s^{-1}. There is no direct link between the MER and the volcanic explosivity index (VEI, Newhall and Self (1982)), but the range of MER used roughly corresponds to VEI 3-7. We set the vent altitude, exit Richardson number, temperature and gas content to 1500 m, -3.16×10^{-2}, 1200 K and 4wt.%, respectively. These values fall in the middle of the range typically observed for explosive eruptions (Aubry et al., 2017).

Atmospheric profiles are retrieved from experiments of the Coupled Model Intercomparison Project Phase 5 (CMIP5) from the MPI-ESM-LR climate model (Giorgetta et al., 2013). Atmospheric profiles are spatially averaged for Iceland (63-67°N,14-24°W) and Philippines (12.5-17.5°N, 121-126°E) to compare the plume models in a tropical and extra-tropical setting. Profiles are also temporally averaged for three 20-year periods: 1981-2000, retrieved from the historical experiment, and 2081-2100 and 2281-2300, retrieved from the RCP8.5 experiment, i.e. the upper-end greenhouse gas emission trajectory in CMIP5 (Van Vuuren et al., 2011). All atmospheric profiles used are provided in Table S1. Compared to 1981-2000, the temperature at 1000 hPa is ca. 3 K and 7.5 K higher in 2081-2100 and 2281-2300, respectively. The tropopause altitude is calculated by finding the lowest altitude at which the temperature lapse rate is less than $2 \mathrm{K km}^{-1}$, for at least 2 km.

Altogether, we run 60 simulations with each plume model corresponding to 10 MERs, 2 locations, and 3 climate scenarios. This experimental design does not allow to extensively explore the impacts of climate change on plume rise for, e.g., different regions and climate scenarios. We also do not explore uncertainties related to the climate model used and weather variability nor different configurations of the 1D (e.g. entrainment parameterization) or 3D (e.g. subgrid turbulence model) plume models. However, these aspects are comprehensively explored either with the 1D plume model in Aubry et al. (2016) or with the 3D model in Cerminara, Ongaro, and Berselli (2016). Our main goal is to assess whether 1D and 3D model agree on changes in plume dynamics induced by climate change, on the basis of 60 representative experiments which already represents an important computational cost for the 3D model.

4 Results

4.1 Plume spreading height

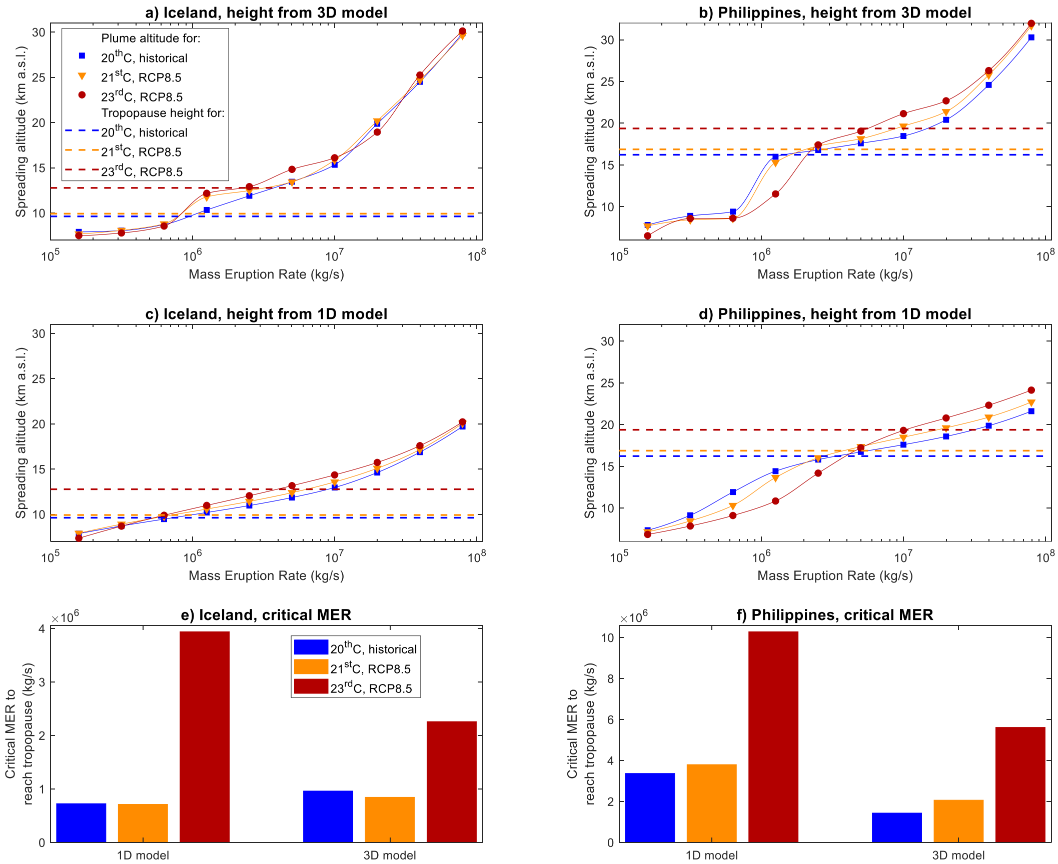

Figure 2. Left and right panels show results for Iceland and the Philippines, respectively. Panels a-d: Plume spreading altitude (km above sea level, a.s.l.) as a function of the MER as predicted by the 3D (a,b) and 1D (c,d) plume models under different climate scenarios. Continuous lines show cubic interpolation of simulation results (symbols). Horizontal dashed lines show the tropopause height for each location/scenario. Panels e-f: Critical MER for which the spreading altitude equates the tropopause, for each scenario and model.

Figure 2 (a-d) shows the spreading altitude of the umbrella cloud as a function of the MER as predicted by the 3D (a,b) and 1D (c,d) plume models for Icelandic (left) and Philippinian (right) atmospheric profiles, for the three climate scenarios used. Both 3D and 1D models show the same trends as the atmospheric profiles change. In Iceland, both models predict an increase in plume height by ca. 1-2 km for MERs between 10^6 and 10^7 kg s^{-1}, going from the 20$^{\text{th}}$ century to the 23$^{\text{rd}}$ century case. In the Philippines, both models predict a decrease in plume height by up to ca. 5km for MERs up to ca. 3×10^6 kg s^{-1} and, above, an increase in plume height by ca. 2km.

Using 12 volcanic areas, (Aubry et al., 2016) show that the trends from Figure 2 for the Philippines are systematic in tropical regions and related to changes in the stratification of the tropical atmosphere. In contrast, changes in plume heights for high-latitude regions, such as Iceland, are more specific to the region considered as they are largely affected by projected changes in both stratification and wind speed profiles.

In addition to plume height, the tropopause height (horizontal dashed lines on Figure 2.a-d) is changing as well. For example, in Iceland and for a MER of 1.25×10^6 kg s^{-1}, the 3D model predicts an increase in plume height by 2km between the historical and RCP8.5 23rd century climate conditions. However, because the tropopause height increases by over 3km between these scenarios, the plume height switches from above the tropopause to below the tropopause. In the Philippines, both decreasing plume height for MERs up to 3×10^6 kg s^{-1} and increasing tropopause height contribute to increase the critical MER required to reach the tropopause as climate changes, shown on Figure 2.e-f. In the Philippines (Figure 2.f) this critical MER increases by 13% (1D model) to 44% (3D model) from a historical climate to a RCP8.5 21st century climate, and by 200% (1D model) to 300% (3D model) from a historical climate to a 23rd century climate.

Figure 2 also reveals quantitative differences between the predictions of the two models. First, for MERs$> 3 \times 10^6$ kg s^{-1}, the 3D model systematically predict higher plume heights than the 1D model (with a 1-10 km difference). Second, for MERs around 10^6 kg s^{-1}, the slope of the plume height-MER curves are much steeper in the 3D model. This affects the model-predicted impact of climate change on plume height. For example, in the Philippines, the critical MER required to reach the tropopause is higher by up to 100% in the 1D model compared to the 3D model.

4.2 Stratospheric injections

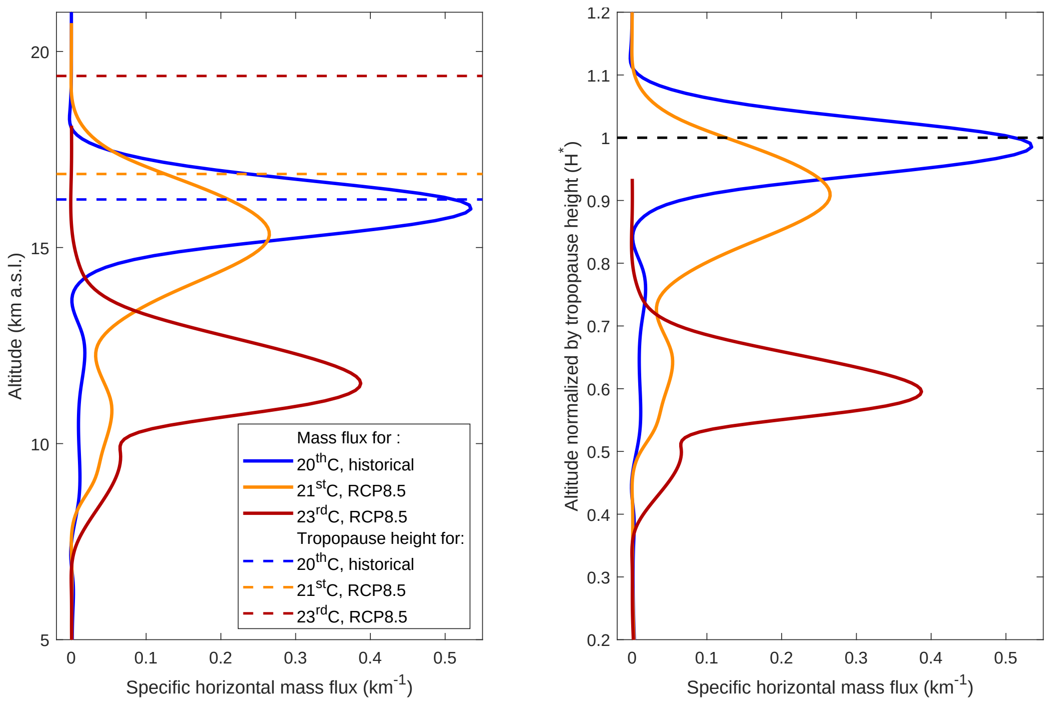

Figure 3. Left: Specific horizontal mass flux profiles as a function of height, as predicted by the 3D model for the Philippines for a MER of 1.25×10^6 kg s^{-1} for the three climate scenarios used. Dashed lines show corresponding tropopause altitudes.
Right: Same as left panel but with the mass flux profile shown as the function of H^*, the ratio of the spreading to tropopause altitude. The horizontal dashed line shows the tropopause ($H^* = 1$).

Whereas Aubry et al. (2016) could only compare predicted plume height to tropopause height to infer changes in stratospheric injections from 1D model simulations, we can investigate changes in the horizontal mass flux profiles in the plume predicted by the 3D model. Figure 3 (left) shows these profiles for the three climate scenarios investigated, for a MER of 1.25×10^6 kg s^{-1} in the Philippines. As expected from Figure 2, the peak of these profiles, which is defined as our spreading height, decreases in height from historical to RCP8.5 climate. With changing tropopause height, horizontal mass flux profiles in the umbrella plotted as a function of H^* (altitude normalized by tropopause height) instead of the altitude are more insightful (Figure 3, right). In the Philippines, both the shift of mass flux profiles to lower altitudes and increase in tropopause height contribute to shifting injections well below the tropopause for the chosen case. We can calculate the fraction of mass injected by the umbrella cloud above the tropopause (F^*) as the ratio of the integral of the mass flow rate above $H^* = 1$ and that of the integral above the vent altitude. For the MER shown in Figure 3, F^* goes from 34% for the historical climate to 8% for the 21$^{\mathrm{st}}$C RCP8.5 climate and 0% for the 23$^{\mathrm{rd}}$C RCP8.5 climate, showing a dramatic decrease of stratospheric inputs for such eruption intensity.

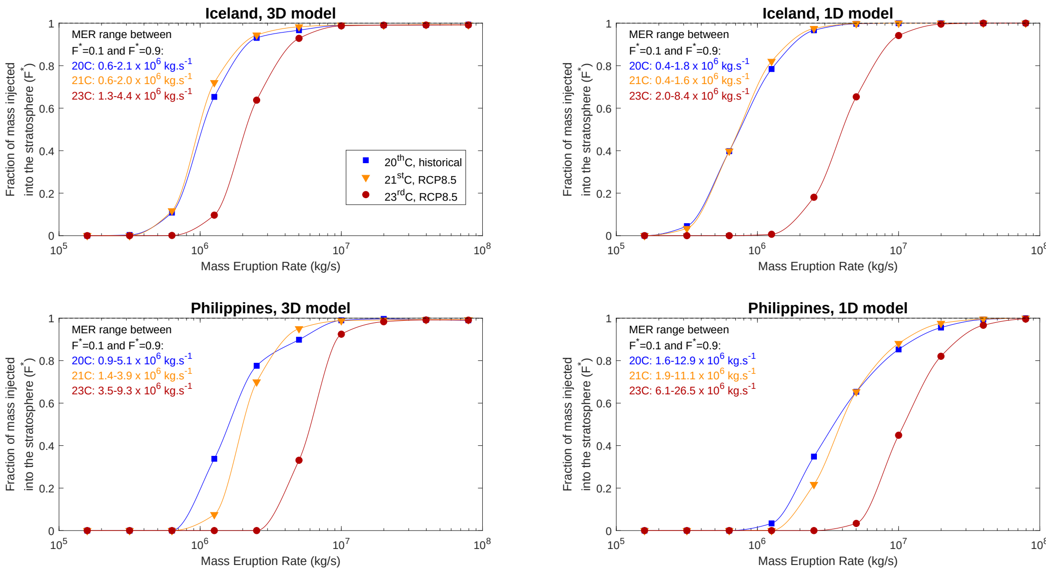

Figure 4. Fraction of mass injected into the stratosphere F^*, calculated by integrating specific horizontal mass flux profiles, as a function of the MER. Panel organization and legend are the same Figure 2.a-d.

Figure 4 (left) shows F^* as a function of the MER for all experiments run in the 3D model in Iceland (top) and the Philippines (bottom). We also report the range of MER for which F^* is between 0.1 and 0.9 on each panel. In Iceland (top left of Fig. 4), F^* is sensitive to climate conditions for MERs between 6×10^5 and 4.4×10^6 kg s^{-1}. Differences between the historical and 21$^{\mathrm{st}}$C RCP8.5 scenario tested are minor because the upward shift of injection profile is mostly compensated by the rise of the tropopause. However, for the 23$^{\mathrm{rd}}$C RCP8.5 scenario, the large increase in tropopause height results in values of F^* smaller by up to 60% compared to the historical scenario. In the Philippines (bottom left of Figure 4), F^* values are sensitive to the climate scenario tested for MERs between 9×10^5 and 9×10^6 kg s^{-1} . The combined downward shifts of injection profile and upward shift of tropopause height mostly results in a decrease of F^*. From a historical to a 21$^{\mathrm{st}}$C RCP8.5 climate scenario, F^* decreases by up to 30% although there is a small range of MERs for which F^* increases by up to 7%. From a historical to a 23$^{\mathrm{rd}}$C

RCP8.5 climate scenario, F^* decreases by up to 80%. In particular, over a range of MERs covering almost an order of magnitude, F^* is smaller by 20-80%.

Rigorously, changes in the mass fraction injected into the stratosphere F^* cannot be investigated with the 1D model. However, if we center and normalize altitude by the spreading height, all individual injection profiles from the 3D model are well fitted by a single gaussian function (Figure S2). As a first-order approximation, we thus use the NBL predicted by the 1D model and the gaussian function shown on Figure S2 to infer an injection profile from the 1D model simulations and calculate the corresponding value of F^*. Results are shown on the right panels of Figure 4. Overall, the trends projected by the 1D models for F^* are in good agreement with those from the 3D model, although some differences exist. For example, in Iceland (top panels of Figure 4), the range of MERs for which F^* is sensitive to climate scenario with the 1D model ($4\times10^5-8\times10^6$ kg s^{-1}) is narrower in the 3D model, which is consistent with the steeper plume height-MER slope of the 3D model highlighted in Figure 2 (a-d).

5 Discussion

5.1 Differences between 1D and 3D plume model projections

Overall, the 1D and 3D plume models agree well on trends in plume height with projected climate change, and in particular that:

- Tropical eruptions whose plume currently reach the lowermost stratosphere will be confined to the troposphere.
- Tropical eruptions whose plume currently reach the lower-middle stratosphere will see their plume height increase by up to a few kilometers.

However, for MERs on the order of 10^6 kg s^{-1}, the 3D model shows a much steeper increase in plume height with increasing MER compared to the 1D model. One potential explanation lies in the double umbrella cloud structure seen in some of the 3D model runs, with two clear local maxima in the horizontal specific mass flow rate profiles (e.g. Figures 3 and S2). When increasing the MER, the height of these local maxima increase. In addition, the largest maxima may switch from the peak located at a lower height to that relatively higher, i.e. the primary umbrella cloud may switch from the lower intrusion height to the higher one. In such case, given our definition of the umbrella cloud spreading height as the height where the maximum horizontal specific mass flow rate is reached, there is a particularly steep increase in spreading height related to both the increasing MER and the switch in the “dominant” umbrella cloud.

In addition, for a MER of 8×10^7 kg s^{-1}, the 3D model (ASHEE) predicts plume heights higher than the 1D model by up to 10 km (Figure 2.a-d). The NBL height (22 km) and maximum height (50 km) obtained for this MER with ASHEE are also high compared to results of the same model for the strong plume case of the eruptive column model inter-comparison study (Costa et al. (2016), MER = 1.5×10^9 kg s^{-1}, and NBL = 22 km/maximum height = 37 km for ASHEE). However, the strong plume simulated for the intercomparison study had smaller exit velocities (275 m s^{-1} instead of 330m s^{-1}), temperature (1053 K instead of 1200 K), and was partially collapsing which likely explain these differences. Note that despite the more realistic treatment of plume dynamics in 3D models, no study has yet taken advantage of recent eruption source parameter datasets (e.g. Mastin (2014); Aubry et al. (2017)) to test whether 3D models provide significantly better predictions than 1D models for the relationship between MER, atmospheric conditions and plume height.

Last, one factor that is not accounted for in this study is how atmospheric humidity impacts the rise of volcanic plumes. Figure S3 shows that when using the 1D model with a value of the condensation rate of 10^{-1} s^{-1} (equivalent to immediate condensation of entrained atmospheric water vapor, Glaze et al. (1997)), the projected changes in plume height for tropical tropospheric eruptions are affected. However, Aubry and Jellinek (2018) show that the plume height predictions of the 1D model used are significantly better when ignoring the effect of condensation. Clarifying the role of water condensation for future eruption dynamics will thus require to incorporate water phase changes and their impacts on the plume buoyancy flux in ASHEE, which is beyond the scope of this study.

5.2 Implications of our results for climate-volcano feedback

All in all, 3D plume model simulations support the core results previously suggested on the basis on 1D plume model simulations. Projected climate change implies a decrease of the height at which tropical volcanic plumes inject gases in the upper troposphere to lowermost stratosphere, and an increase of plume height in the low-mid stratosphere. In addition to validating these results, our new numerical experiments demonstrate that combined changes in plume height and tropopause height should result in reduced stratospheric gas injections for a large range of eruption intensities. To illustrate the consequences of our results, we use an idealized box model of volcanic aerosol forcing to predict the global mean stratospheric aerosol optical depth (SAOD) timeseries for each experiment we conducted. This model (preliminary version published in Aubry (2018)) builds on the Easy Volcanic Aerosol model (Toohey et al., 2016) but accounts for injection height. SO_2 injection profiles are either taken from the 1D or 3D plume model predictions. Table S3 shows the resulting time-integrated SAOD for all experiments.

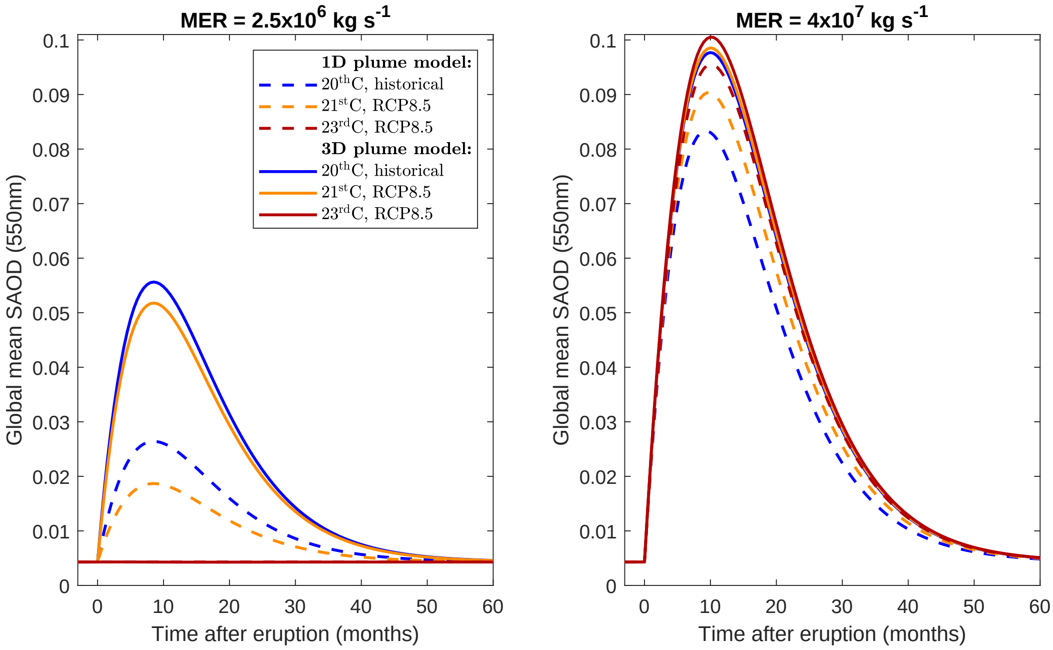

Figure 5. Global mean stratospheric aerosol optical depth (SAOD) timeseries at 550nm projected for an eruption injecting 9TgS into the atmosphere in the Philippines, with a MER of 2.5×10^6 kg s^{-1} (left) or 4×10^7 kg s^{-1} (right). SAOD are predicted by an aerosol box model to which we specify SO_2 injections profile from the 1D (dashed lines) or 3D (continuous lines) plume model. Colors correspond to the climate scenarios used for atmospheric conditions inputted in the plume model.

Figure 5 shows the SAOD timeseries for MERs of 2.5×10^6 kg s^{-1} (left) and 4×10^7 kg s^{-1} (right) in the Philippines. These two cases are particularly relevant to the climate community because they respectively represent upper tropospheric/lower stratospheric tropical eruptions, which govern the stratospheric aerosol background (Solomon et al., 2011; Schmidt et al., 2018), and major mid-stratospheric tropical eruptions, which exert a considerable forcing with decadal impacts on climate variability (Robock, 2000). For the weaker MER (Figure 5, left), we project a decrease of peak SAOD by 7% (3D model) to 29% (1D model) from a present-day climate to a RCP8.5 21^{st}C scenario, and a nihil perturbation of SAOD for a RCP8.5 23^{rd}C scenario. This effect is directly related to the lower mass fraction injected into the stratosphere in RCP8.5 scenario for this MER (Fig. 4). For the stronger MER (Figure 5, right), we project an increase of peak SAOD by up 3% (3D model) to 13% (1D model) in RCP8.5 scenario relative to present-day climate, depending on the plume model used. This effect is related to the higher injection height predicted by the plume models, which results in longer aerosol decay timescales in the aerosol box model.

Although simplistic, our approach illustrates the variety of feedback potentially at play between climate and volcanoes. In particular, it suggests a future decrease in the forcing associated with eruptions currently injecting gases in the uppermost troposphere/lowermost stratosphere, but an increase for mid-stratospheric eruptions. For the latter eruptions, the magnitude of the SAOD increase projected from the aerosol box model compares to decrease in forcing associated with a future Tambora-like eruption in Hopcroft et al. (2017). Figure 5 thus suggests that climate-volcano feedback related to plume dynamics would have climatic implications comparable to feedback related to the sensitivity of the response to volcanic forcing to the background climate (Fasullo et al., 2017; Hopcroft et al., 2017). We thus urge future studies on climate-volcano feedback to incorporate the impact of climate changes on the vertical distribution of volcanic gases in the atmosphere. For specific case studies, e.g. future Tambora-like eruption (Fasullo et al., 2017; Hopcroft et al., 2017), 3D plume models can be used for a more complex and physical representation of the dynamics of umbrella cloud. For studies exploring the effect of future eruption sequences (e.g. Bethke et al. (2017)) the cost of 3D plume models is prohibitive but 1D models with parameterized injection profiles (Figure S2) can be used and our study demonstrates that their projections for trends in future plume height and stratospheric injections are comparable to 3D models.

6 Conclusions

We use a 1D and a 3D volcanic plume model to assess the potential impacts of ongoing climate change on the rise of explosive volcanic columns. We demonstrate that climate change may affect the vertical distribution of SO_2 injected by future eruptions into the atmosphere. In particular, both models agrees on two trends for tropical eruptions:

- Higher eruption intensities will be required for plumes to reach the upper troposphere/lower stratosphere. This is a consequence of both a decrease of plume height in this region and an increase of the tropopause height.
- The height of plumes currently reaching the lower stratosphere or above will increase.

Using an idealized volcanic aerosol box model, we show that these changes in plume dynamics would affect post-eruption SAOD. Our results thus demonstrate that an approach from the vent onward is required to understand how climate change will affect future eruptions and their climatic impacts. As a consequence, four classes of climate-volcano feedback governing the climatic impacts of a future eruptions can be identified:

1. Feedback affecting eruption source conditions, such as the impact of deglaciation on the frequency-magnitude distribution of eruptions (e.g. Cooper et al. (2018)).
2. Feedback related to plume dynamics and SO_2 injection into the atmosphere (Aubry et al. (2016), this study).
3. Feedback related to volcanic sulfate aerosol chemistry and microphysics (Mills et al., 2016; Kremser et al., 2016), which remain unexplored. As an example, would SO_2-sulfate aerosol conversion rate be modulated by the ongoing cooling of the stratosphere?
4. Feedback modulating Earth's radiative balance and climate response to a specified distribution of volcanic aerosols, e.g. as a consequence of changes in tropospheric aerosols (Hopcroft et al., 2017) and ocean stratification (Fasullo et al., 2017).

Understanding how these feedback combine together will enable to better understand the climatic impact of future volcanic explosive eruptions.

The large panel of numerical experiments we conducted also sheds new lights on differences between 1D and 3D plume models (Costa et al., 2016). In particular, despite a good agreement on trends in plume height with ongoing climate change, the models show differences in the predicted relationship between the MER and the plume height, both under tropical and extra-tropical atmospheric conditions (Section 5.1). We also show that 3D models can inform a simple parameterization of the shape of the umbrella cloud that can then be used to predict injection profiles from NBL predictions of a 1D plume model.

Acknowledgments

We sincerely thank the editor, Gudrun Magnusdottir, and two anonymous reviewers whose comments improved the manuscript. T.J.A. acknowledges funding from the Royal Society through a Newton International Fellowship (grant number NIF\R1\180809). M.C. acknowledges: CINECA award N. HP10BRDK2T (2017) for high performance computing resources used for testing the ASHEE code; the FISR 2016 "Centro di studio e monitoraggio dei rischi naturali dell'Italia centrale" project framework, managed by the Italian National Institute of Geophysics and Volcanology (INGV) and funded by the Italian Ministry of Education, University and Research; and the European Union's Horizon 2020 research and innovation programme under grant agreement No 731070. T.J.A. and A.M.J. acknowledge support by the Natural Sciences and Engineering Research Council of Canada during completion of this work. We acknowledge the World Climate Research Programme's Working Group on Coupled Modeling, which is responsible for CMIP, and we thank Max Planck Institut climate modeling groups for producing and making available the MPI-ESM model output. Atmospheric data used in this study are available in Table S1. Plume heights from all simulations conducted for this study are available in Table S2.

References

Aubry, T. J. (2018). *Interactions between climate and the rise of explosive volcanic plumes: a new feedback in the earth system.* (Unpublished doctoral dissertation). University of British Columbia.

Aubry, T. J., & Jellinek, A. M. (2018). New insights on entrainment and condensation in volcanic plumes: Constraints from independent observations of explosive eruptions and implications for assessing their impacts. *Earth and Planetary Science Letters*, *490*, 132 - 142. doi: https://doi.org/10.1016/j.epsl.2018.03.028

Aubry, T. J., Jellinek, A. M., Carazzo, G., Gallo, R., Hatcher, K., & Dunning, J. (2017). A new analytical scaling for turbulent wind-bent plumes: Comparison of scaling laws with analog experiments and a new database of eruptive conditions for predicting the height of volcanic plumes. *Journal of Volcanology and Geothermal Research*. doi: 10.1016/j.jvolgeores.2017.07.006

Aubry, T. J., Jellinek, A. M., Degruyter, W., Bonadonna, C., Radić, V., Clyne, M., & Quainoo, A. (2016). Impact of global warming on the rise of volcanic plumes and implications for future volcanic aerosol forcing. *Journal of Geophysical Research: Atmospheres*, *121*(22), 13,326–13,351. doi: 10.1002/2016JD025405

Bardina, J., Ferziger, J., & Reynolds, W. (n.d.). Improved subgrid-scale models for large-eddy simulation. In *13th fluid and plasmadynamics conference*. Retrieved from `https://arc.aiaa.org/doi/abs/10.2514/6.1980-1357` doi: 10.2514/6.1980-1357

Bethke, I., Outten, S., Otterå, O. H., Hawkins, E., Wagner, S., Sigl, M., & Thorne, P. (2017). Potential volcanic impacts on future climate variability. *Nature Climate Change*, *7*(11), 799. doi: 10.1038/nclimate3394

Bursik, M. (2001). Effect of wind on the rise height of volcanic plumes. *Geophysical Research Letters*, *28*, 3821-3824. doi: 10.1029/2001GL013393

Cerminara, M., Ongaro, T. E., & Berselli, L. C. (2016). Ashee-1.0: a compressible, equilibrium–eulerian model for volcanic ash plumes. *Geoscientific Model Development*, *9*(2), 697–730. Retrieved from `https://www.geosci-model-dev.net/9/697/2016/` doi: 10.5194/gmd-9-697-2016

Cerminara, M., Ongaro, T. E., & Neri, A. (2016). Large eddy simulation of gas–particle kinematic decoupling and turbulent entrainment in volcanic plumes. *Journal of Volcanology and Geothermal Research*, *326*, 143 - 171. Retrieved from `http://www.sciencedirect.com/science/article/pii/S0377027316301688` doi: https://doi.org/10.1016/j.jvolgeores.2016.06.018

Cooper, C. L., Swindles, G. T., Savov, I. P., Schmidt, A., & Bacon, K. L. (2018). Evaluating the relationship between climate change and volcanism. *Earth-Science Reviews*, *177*, 238 - 247. Retrieved from `http://www.sciencedirect.com/science/article/pii/S0012825217301629` doi: https://doi.org/10.1016/j.earscirev.2017.11.009

Costa, A., Suzuki, Y., Cerminara, M., Devenish, B., Ongaro, T. E., Herzog, M., ... Bonadonna, C. (2016). Results of the eruptive column model intercomparison study. *Journal of Volcanology and Geothermal Research*. doi: 10.1016/j.jvolgeores.2016.01.017

Degruyter, W., & Bonadonna, C. (2012). Improving on mass flow rate estimates of volcanic eruptions. *Geophysical Research Letters*, *39*(16). doi: 10.1029/2012GL052566

Devenish, B. J., & Cerminara, M. (2018). The transition from eruption column to umbrella cloud. *Journal of Geophysical Research: Solid Earth*, *123*(12), 10,418-10,430. doi: 10.1029/2018JB015841

Fasullo, J., Tomas, R., Stevenson, S., Otto-Bliesner, B., Brady, E., & Wahl, E. (2017). The amplifying influence of increased ocean stratification on a future year without a summer. *Nature Communications*, *8*(1), 1236. doi: 10.1038/s41467-017-01302-z

Giorgetta, M. A., Jungclaus, J., Reick, C. H., Legutke, S., Bader, J., Böttinger, M., ... others (2013). Climate and carbon cycle changes from 1850 to 2100 in MPI-ESM simulations for the Coupled Model Intercomparison Project phase 5. *Journal of Advances in Modeling Earth Systems*, *5*(3), 572–597. doi: 10.1002/jame.20038

Glaze, L. S., Baloga, S. M., & Wilson, L. (1997). Transport of atmospheric water vapor by volcanic eruption columns. *Journal of Geophysical Research: Atmospheres*, *102*(D5), 6099–6108. Retrieved from `10.1029/96JD03125` doi: 10.1029/96JD03125

Hopcroft, P. O., Kandlbauer, J., Valdes, P. J., & Sparks, R. S. J. (2017). Reduced cooling following future volcanic eruptions. *Climate Dynamics*. doi: 10.1007/

s00382-017-3964-7

Hoult, D., Fay, J., & Forney, L. (1969). A theory of plume rise compared with field observations. *Journal of the Air Pollution Control Association*, *19*, 585-590. doi: 10.1080/00022470.1969.10466526

Jellinek, A. M., Manga, M., & Saar, M. O. (2004). Did melting glaciers cause volcanic eruptions in eastern California? Probing the mechanics of dike formation. *Journal of Geophysical Research: Solid Earth*, *109*(B9). (B09206) doi: 10.1029/2004JB002978

Kremser, S., Thomason, L. W., von Hobe, M., Hermann, M., Deshler, T., Timmreck, C., ... Meland, B. (2016). Stratospheric aerosol—observations, processes, and impact on climate. *Reviews of Geophysics*, *54*(2), 278-335. Retrieved from `https://agupubs.onlinelibrary.wiley.com/doi/abs/10.1002/2015RG000511` doi: 10.1002/2015RG000511

Mastin, L. (2014). Testing the accuracy of a 1-D volcanic plume model in estimating mass eruption rate. *Journal of Geophysical Research: Atmospheres*, *119*(5), 2474–2495. doi: 10.1002/2013JD020604

Mills, M. J., Schmidt, A., Easter, R., Solomon, S., Kinnison, D. E., Ghan, S. J., ... Gettelman, A. (2016). Global volcanic aerosol properties derived from emissions, 1990–2014, using CESM1 (WACCM). *Journal of Geophysical Research: Atmospheres*, *121*(5), 2332–2348. doi: 10.1002/2015JD024290

Moin, P., Squires, K., Cabot, W., & Lee, S. (1991). A dynamic subgrid-scale model for compressible turbulence and scalar transport. *Physics of Fluids A: Fluid Dynamics*, *3*(11), 2746-2757. Retrieved from `https://doi.org/10.1063/1.858164` doi: 10.1063/1.858164

Morton, B. R. (1959). Forced plumes. *Journal of Fluid Mechanics*, *5*(1), 151–163. doi: 10.1017/S002211205900012X

Morton, B. R., Taylor, G., & Turner, J. S. (1956). Turbulent gravitational convection from maintained and instantaneous sources. *Proceedings of the Royal Society of London A: Mathematical, Physical and Engineering Sciences*, *234*(1196), 1–23. doi: 10.1098/rspa.1956.0011

Newhall, C. G., & Self, S. (1982). The Volcanic Explosivity Index (VEI): an estimate of explosive magnitude for historical volcanism. *Journal of Geophysical Research*, *87*, 1231-1238. doi: 10.1029/JC087iC02p01231

Robock, A. (2000). Volcanic eruptions and climate. *Reviews of Geophysics*, *38*, 191-219. doi: 10.1029/1998RG000054

Santer, B., Bonfils, C., Painter, J., Zelinka, M., Mears, C., Solomon, S., ... Wentz, F. (2014). Volcanic contribution to decadal changes in tropospheric temperature. *Nature Geoscience*, *7*, 185-189. doi: 10.1038/ngeo2098

Schmidt, A., Mills, M. J., Ghan, S., Gregory, J. M., Allan, R. P., Andrews, T., ... Toon, O. B. (2018). Volcanic radiative forcing from 1979 to 2015. *Journal of Geophysical Research: Atmospheres*, *123*(22), 12,491-12,508. doi: 10.1029/2018JD028776

Sigl, M., Winstrup, M., McConnell, J., Welten, K., Plunkett, G., Ludlow, F., ... Woodruff, T. E. (2015). Timing and climate forcing of volcanic eruptions for the past 2,500 years. *Nature*.

Smagorinsky, J. (1963). General circulation experiments with the primitive equations. *Monthly Weather Review*, *91*(3), 99-164. doi: 10.1175/1520-0493(1963)091⟨0099:GCEWTP⟩2.3.CO;2

Solomon, S., Daniel, J. S., Neely, R. R., Vernier, J.-P., Dutton, E. G., & Thomason, L. W. (2011). The persistently variable "background" stratospheric aerosol layer and global climate change. *Science*, *333*(6044), 866–870. doi: 10.1126/science.1206027

Suzuki, Y. J., & Koyaguchi, T. (2009). A three-dimensional numerical simulation of spreading umbrella clouds. *Journal of Geophysical Research: Solid Earth*, *114*(B3). Retrieved from `https://agupubs.onlinelibrary.wiley.com/doi/`

abs/10.1029/2007JB005369 doi: 10.1029/2007JB005369

Toohey, M., Stevens, B., Schmidt, H., & Timmreck, C. (2016). Easy Volcanic Aerosol (EVA v1.0): An idealized forcing generator for climate simulations. *Geoscientific Model Development Discussions*, *2016*, 1–40. doi: 10.5194/gmd-2016-83

Van Vuuren, D., Edmonds, J., Kainuma, M., Riahi, K., Thomson, A., Hibbard, K., ... Rose, S. (2011). The representative concentration pathways: an overview. *Climatic Change*, *109*(1-2), 5-31. Retrieved from 10.1007/s10584-011-0148-z doi: 10.1007/s10584-011-0148-z

Watt, S. F., Pyle, D. M., & Mather, T. A. (2013). The volcanic response to deglaciation: Evidence from glaciated arcs and a reassessment of global eruption records. *Earth-Science Reviews*, *122*, 77 - 102. Retrieved from http://www.sciencedirect.com/science/article/pii/S0012825213000664 doi: https://doi.org/10.1016/j.earscirev.2013.03.007

Woods, A. (1988). The fluid dynamics and thermodynamics of eruption columns. *Bulletin of Volcanology*, *50*(3), 169–193. doi: 10.1007/BF01079681

Woods, A. (1995). The dynamics of explosive volcanic eruptions. *Review of Geophysics*, *33*, 496-530. doi: 10.1029/95RG02096